Dynamical mean-field theory within an augmented plane-wave framework: Assessing electronic correlations in the iron pnictide LaFeAsO

Markus Aichhorn,[1] Leonid Pourovskii,[1] Veronica Vildosola,[1,2,3] Michel Ferrero,[1,4] Olivier Parcollet,[4] Takashi Miyake,[3,5,6] Antoine Georges,[1,3,7] and Silke Biermann[1,3]

[1]*Centre de Physique Théorique, École Polytechnique, CNRS, 91128 Palaiseau Cedex, France*

[2]*Departamento de Física, Comisión Nacional de Energía Atómica (CNEA–CONICET), Provincia de Buenos Aires, San Martín, 1650, Argentina*

[3]*Japan Science and Technology Agency, CREST, Kawaguchi 332-0012, Japan*

[4]*Institut de Physique Théorique, CEA/DSM/IPhT-CNRS/URA 2306, CEA–Saclay, F-91191 Gif-sur-Yvette, France*

[5]*Research Institute for Computational Sciences, AIST, Tsukuba 305-8568, Japan*

[6]*Japan Science and Technology Agency, TRIP, Kawaguchi 332-0012, Japan*

[7]*Collège de France, 11 Place Marcelin Berthelot, 75231 Paris Cedex 05, France*

(Received 23 June 2009; revised manuscript received 10 July 2009; published 3 August 2009)

We present an approach that combines the local-density approximation (LDA) and the dynamical mean-field theory (DMFT) in the framework of the full-potential linear augmented plane-wave method. Wannier-type functions for the correlated shell are constructed by projecting local orbitals onto a set of Bloch eigenstates located within a certain energy window. The screened Coulomb interaction and Hund's coupling are calculated from a first-principles constrained random-phase approximation scheme. We apply this LDA+DMFT implementation, in conjunction with a continuous-time quantum Monte Carlo algorithm, to the study of electronic correlations in LaFeAsO. Our findings support the physical picture of a metal with intermediate correlations. The average value of the mass renormalization of the Fe 3*d* bands is about 1.6, in reasonable agreement with the picture inferred from photoemission experiments. The discrepancies between different LDA+DMFT calculations (all technically correct) which have been reported in the literature are shown to have two causes: (i) the specific value of the interaction parameters used in these calculations and (ii) the degree of localization of the Wannier orbitals chosen to represent the Fe 3*d* states, to which many-body terms are applied. The latter is a fundamental issue in the application of many-body calculations, such as DMFT, in a realistic setting. We provide strong evidence that the DMFT approximation is more accurate and more straightforward to implement when well-localized orbitals are constructed from a large energy window encompassing Fe-3*d*, As-4*p*, and O-2*p* and point out several difficulties associated with the use of extended Wannier functions associated with the low-energy iron bands. Some of these issues have important physical consequences regarding, in particular, the sensitivity to the Hund's coupling.

DOI: 10.1103/PhysRevB.80.085101 PACS number(s): 71.15.Mb, 71.10.Fd, 71.20.Be, 74.70.−b

I. INTRODUCTION

This paper has two purposes. The first one is to present an implementation of dynamical mean-field theory (DMFT) within electronic structure calculation methods. This implementation is based on a highly precise full-potential linear augmented plane-wave (FLAPW) method, as implemented in the WIEN2K electronic structure code.[1] The second purpose of this paper is to report on DMFT calculations for the iron oxypnictide LaFeAsO, the parent compound of the "1111"-family of recently discovered iron-based superconductors. The strength of electronic correlations in these materials is an important issue, which has been a subject of debate in the literature.[2–6]

The combination of dynamical mean-field theory with density-functional theory in the local-density approximation (LDA+DMFT) provides a powerful framework for the quantitative description of electronic correlations in a realistic setting. A number of materials have been investigated in this framework over the past decade, such as transition metals and transition-metal oxides, rare-earth and actinide compounds, and organic conductors. These examples testify to the progress in our understanding of the key physical phenomena associated with the competition between the localized and itinerant characters of electrons belonging to different orbitals (see, e.g., Refs. 7–12 for reviews).

In the past few years, a new generation of LDA+DMFT implementations have been put forward,[13–19] which emphasize the use of Wannier functions as a natural bridge between the band-structure and the real-space description of the solid in terms of orbitals. These functions span the subset of orbitals which are treated within the many-body DMFT framework. In this paper, we present an implementation of LDA+DMFT within the FLAPW framework, using atomic orbitals that are promoted to Wannier functions by a truncated expansion over Bloch functions followed by an orthonormalization procedure. This is a simpler alternative to the previous implementation of DMFT within FLAPW,[14] which constructed the Wannier functions following the prescription of maximal localization.[20,21] The choice of FLAPW is motivated by the high level of accuracy of this all-electron, full-potential method. In the present work, we use the WIEN2K electronic structure package[1] and we have constructed an interface to it that allows for the construction of Wannier-type functions used in DMFT. Our implementation is described in detail in Sec. II. As a benchmark, we perform

 ©2009 The American Physical Society

calculations on a test material, $SrVO_3$, which are presented in Appendix A and compared to previously published results for this material.[13,17,22–26] Throughout this paper, many-body effects are treated in the DMFT framework using the recently developed continuous-time strong-coupling quantum Monte Carlo algorithm of Werner and co-workers.[27,28] Because very low temperatures can be reached, and very high accuracy can be obtained at low frequency, this algorithm represents a major computational advance in the field.

In Sec. III, we address the issue of electronic correlations in LaFeAsO. The DMFT calculations which have been published soon after the experimental discovery of superconductivity in the iron oxypnictides have provided seemingly contradictory answers to this question. In Refs. 2 and 3, Haule and Kotliar proposed that LaFeAsO is a strongly correlated metal, rather close to the Mott metal-insulator transition, and characterized by a reduced value of the quasiparticle coherence scale, resulting in bad metallic behavior. In contrast, in Refs. 4–6, Anisimov and co-workers proposed that these materials are in a weak to intermediate regime of correlations.

Our LDA+DMFT calculations for LaFeAsO support the physical picture of a metal with intermediate correlations. The average value of the mass renormalization of the Fe 3*d* bands is about 1.6, in reasonable agreement with the picture inferred from photoemission experiments. We also find that there is no technical inconsistency between different DMFT results reported for LaFeAsO before. We show that the discrepancies in the literature are due to two causes: (i) the specific value of the interaction parameters used in these calculations and (ii) the degree of localization of the Wannier orbitals chosen to represent the Fe 3*d* states, to which many-body terms are applied.

In Sec. III, we perform detailed comparisons between LDA+DMFT calculations performed with different degree of localization of the correlated orbitals, associated with different choices of energy windows for the Wannier construction (and accordingly, different degrees of screening of the interaction parameters). We point out several difficulties associated with the use of more extended Wannier functions associated with the low-energy iron bands only. Some of these issues have important physical consequences, in particular regarding the sensitivity to the Hund's coupling.

This paper ends with several appendices, reporting on more detailed aspects or technical issues. Appendix A is devoted to a benchmark of our implementation on a "classical" test compound, $SrVO_3$. Appendix B details some technical issues associated with the projection scheme used to display partial spectral functions with a given orbital character. Appendix C discusses the influence of spin-flip and pair-hopping terms on the degree of correlations on the basis of model calculations. We conclude that while these terms are indeed important close to the Mott transition, they can safely be neglected in the regime of correlations relevant to LaFeAsO.

II. THEORETICAL FRAMEWORK

A. Implementation of LDA+DMFT in the APW framework

1. LDA+DMFT in the basis of Bloch waves

To make this paper self-contained and in order to define the main notations, this subsection begins by briefly reviewing some essential aspects of the LDA+DMFT framework. The presentation is close to that of Refs. 14 and 19, where additional details can be found.

Dynamical mean-field theory is a quantitative method for handling electron correlations, which can be described as an "effective atom" approach. The self-energy in the solid is approximated by that of a local model, a generalized Anderson impurity model describing a specific set of atomiclike orbitals coupled to a self-consistent environment. The self-consistency requirement is that the local on-site Green's function of the solid, calculated using this local self-energy, must coincide with the Green's function of the effective impurity model.

In order to formulate the local effective atom problem, a set of (orthonormal) local orbitals $|\chi_m^{\alpha,\sigma}\rangle$, and corresponding Wannier-type functions $|w_{\mathbf{k}m}^{\alpha,\sigma}\rangle$, must be constructed. These Wannier functions span the "correlated" subspace $\mathcal{C}$ of the full Hilbert space, in which many-body correlations [beyond local-density approximation (LDA)] are taken into account. This set of orbitals spanning the correlated subspace must be clearly distinguished from the full basis set of the problem, in which the Green's function of the solid can be expressed. Obviously, the basis set spans a much larger Hilbert space involving all relevant electronic shells.

Below, we discuss in details how the $|w_{\mathbf{k}m}^{\alpha,\sigma}\rangle$ are constructed from the local orbitals $|\chi_m^{\alpha,\sigma}\rangle$. The index m is an orbital index within the correlated subset, α denotes the atom in the unit cell, and σ is the spin degree of freedom. Projections of quantities of interest on the subset $\mathcal{C}$ are done using the projection operator

$$\hat{P}^{\alpha,\sigma}(\mathbf{k}) = \sum_{m \in \mathcal{C}} |w_{\mathbf{k}m}^{\alpha,\sigma}\rangle\langle w_{\mathbf{k}m}^{\alpha,\sigma}|. \tag{1}$$

The effective impurity model is then constructed for the correlated subset $\mathcal{C}$. It is defined by the Green's function of the effective environment, $\mathcal{G}_{mm'}^{0,\sigma}(i\omega_n)$, and Hubbard-Kanamori interaction parameters $U_{mm'm''m'''}$. By solving this model in a suitably chosen manner one obtains the impurity Green's function $G_{mm'}^{\sigma,\mathrm{imp}}(i\omega_n)$ as well as the impurity self-energy

$$\Sigma_{mm'}^{\sigma,\mathrm{imp}}(i\omega_n) = (\mathcal{G}^{\sigma,0}(i\omega_n))_{mm'}^{-1} - (G^{\sigma,\mathrm{imp}}(i\omega_n))_{mm'}^{-1}. \tag{2}$$

For the formulation of the self-consistency condition relating the lattice Green's function of the solid to the impurity model, it is convenient to choose the Bloch basis $|\psi_{\mathbf{k}\nu}^{\sigma}\rangle$ as the complete basis set of the problem, since it is a natural output of any electronic structure calculation. The (inverse) Green's function of the solid expressed in this basis set is given by

$$G^{\sigma}(\mathbf{k}, i\omega_n)_{\nu\nu'}^{-1} = (i\omega_n + \mu - \epsilon_{\mathbf{k}\nu}^{\sigma})\delta_{\nu\nu'} - \Sigma_{\nu\nu'}^{\sigma}(\mathbf{k}, i\omega_n), \tag{3}$$

where $\epsilon_{\mathbf{k}\nu}^{\sigma}$ are the Kohn-Sham (KS) eigenvalues and $\Sigma_{\nu\nu'}^{\sigma}(\mathbf{k}, i\omega_n)$ is the approximation to the self-energy obtained by the solution of the DMFT impurity problem. It is obtained by "upfolding" the impurity local self-energy as

$$\Sigma^{\sigma}_{\nu\nu'}(\mathbf{k},i\omega_n) = \sum_{\alpha,mm'} P^{\alpha,\sigma*}_{\nu m}(\mathbf{k})\Delta\Sigma^{\sigma,\mathrm{imp}}_{mm'}(i\omega_n)P^{\alpha,\sigma}_{m'\nu'}(\mathbf{k}), \quad (4)$$

where $P^{\alpha,\sigma}_{m\nu}(\mathbf{k})=\langle w^{\alpha,\sigma}_{\mathbf{k}m}|\psi^{\sigma}_{\mathbf{k},\nu}\rangle$ are the matrix elements of the projection operator, Eq. (1) and

$$\Delta\Sigma^{\sigma,\mathrm{imp}}_{mm'}(i\omega_n) = \Sigma^{\sigma,\mathrm{imp}}_{mm'}(i\omega_n) - \Sigma^{\mathrm{dc}}_{mm'}. \quad (5)$$

Here, $\Sigma^{\sigma,\mathrm{imp}}_{mm'}$ is the impurity self-energy, Eq. (2), expressed in the local orbitals, and $\Sigma^{\mathrm{dc}}_{mm'}$ is a double-counting correction, which will be discussed in Sec. II B.

The local Green's function is obtained by projecting the lattice Green's function to the set of correlated orbitals m of the correlated atom α and summing over the full Brillouin zone,

$$G^{\sigma,\mathrm{loc}}_{mm'}(i\omega_n) = \sum_{\mathbf{k},\nu\nu'} P^{\alpha,\sigma}_{m\nu}(\mathbf{k})G^{\sigma}_{\nu\nu'}(\mathbf{k},i\omega_n)P^{\alpha,\sigma*}_{\nu'm'}(\mathbf{k}). \quad (6)$$

Note that the local quantities $G^{\sigma,\mathrm{loc}}_{mm'}(i\omega_n)$ and $\Delta\Sigma^{\sigma,\mathrm{imp}}_{mm'}(i\omega_n)$ carry also an index α, which we suppressed for better readability.

The self-consistency condition of DMFT imposes that the *local* Green's function, Eq. (6), must coincide with the one obtained from the effective impurity problem,

$$\mathbf{G}^{\sigma,\mathrm{loc}}(i\omega_n) = \mathbf{G}^{\sigma,\mathrm{imp}}(i\omega_n). \quad (7)$$

This equation implies that the Green's function of the effective environment, $\mathcal{G}_0$, must be self-consistently related to the self-energy of the impurity model through

$$\mathcal{G}_0^{-1} = \Sigma_{\mathrm{imp}} + G^{-1}_{\mathrm{loc}}, \quad (8)$$

where the dependence of G_{loc} on Σ_{imp} is specified by Eqs. (3) and (6). In practice, the DMFT equations are solved iteratively: starting from an initial $\mathcal{G}_0$, the impurity model is solved for Σ_{imp} and a new $\mathcal{G}_0$ is constructed from Eq. (8). The cycle is repeated until convergence is reached.

In order to construct the set of Wannier functions, we start from a set of local atomiclike orbitals $|\chi^{\alpha,\sigma}_m\rangle$ defined in the unit cell. These orbitals can be expanded over the full Bloch basis set as

$$|\chi^{\alpha,\sigma}_{\mathbf{k}m}\rangle = \sum_{\nu} \langle\psi^{\sigma}_{\mathbf{k}\nu}|\chi^{\alpha,\sigma}_m\rangle|\psi^{\sigma}_{\mathbf{k}\nu}\rangle. \quad (9)$$

This expansion is then truncated by choosing an energy window $\mathcal{W}$ and restricting the sum to those Bloch states with Kohn-Sham energies $\epsilon_{\mathbf{k}\nu}$ within $\mathcal{W}$. The number of bands included in $\mathcal{W}$ will in general depend on $\mathbf{k}$ and σ. We thus define the modified orbitals (which do not form an orthonormal set because of the truncation):

$$|\tilde{\chi}^{\alpha,\sigma}_{\mathbf{k}m}\rangle = \sum_{\nu\in\mathcal{W}} \langle\psi^{\sigma}_{\mathbf{k}\nu}|\chi^{\alpha,\sigma}_m\rangle|\psi^{\sigma}_{\mathbf{k}\nu}\rangle. \quad (10)$$

Let us denote the matrix elements of the projection operator for this subset as

$$\tilde{P}^{\alpha,\sigma}_{m\nu}(\mathbf{k}) = \langle\tilde{\chi}^{\alpha,\sigma}_m|\psi^{\sigma}_{\mathbf{k}\nu}\rangle, \quad \nu\in\mathcal{W}. \quad (11)$$

The matrix $\tilde{P}^{\alpha,\sigma}_{m\nu}(\mathbf{k})$ is not unitary, except when the sum in Eq. (10) is carried over all Bloch bands. It is also important to note that the matrices $\tilde{P}^{\alpha,\sigma}$ are in general nonsquare matrices. They reduce to square matrices only in the case when the number of Kohn-Sham bands contained in the chosen window equals at every $\mathbf{k}$ point the number of correlated local orbitals to be constructed.

The orbitals $|\tilde{\chi}^{\alpha,\sigma}_{\mathbf{k}m}\rangle$ can be orthonormalized giving a set of Wannier-type functions,

$$|w^{\alpha,\sigma}_{\mathbf{k}m}\rangle = \sum_{\alpha',m'} S^{\alpha,\alpha'}_{m,m'}|\tilde{\chi}^{\alpha',\sigma}_{\mathbf{k}m'}\rangle, \quad (12)$$

where $S^{\alpha,\alpha'}_{m,m'}=\{O(\mathbf{k},\sigma)^{-1/2}\}^{\alpha,\alpha'}_{m,m'}$ and $O^{\alpha,\alpha'}_{m,m'}(\mathbf{k},\sigma)=\langle\tilde{\chi}^{\alpha,\sigma}_{\mathbf{k}m}|\tilde{\chi}^{\alpha',\sigma}_{\mathbf{k}m'}\rangle$ the overlap matrix elements.

The overlap $O^{\alpha,\alpha'}_{m,m'}(\mathbf{k},\sigma)$ finally reads

$$O^{\alpha,\alpha'}_{m,m'}(\mathbf{k},\sigma) = \sum_{\mathcal{W}} \tilde{P}^{\alpha,\sigma}_{m\nu}(\mathbf{k})\tilde{P}^{\alpha',\sigma*}_{\nu m'}(\mathbf{k}), \quad (13)$$

while the orthonormalized projectors are then written as

$$P^{\alpha,\sigma}_{m\nu}(\mathbf{k}) = \sum_{\alpha'm'} \{[O(\mathbf{k},\sigma)]^{-1/2}\}^{\alpha,\alpha'}_{m,m'}\tilde{P}^{\alpha',\sigma}_{m'\nu}(\mathbf{k}). \quad (14)$$

2. Augmented plane waves

In this work, the Bloch basis $|\psi^{\sigma}_{\mathbf{k}\nu}\rangle$ are expanded in augmented plane waves (APW/LAPW), which will be briefly described in the following. As was first pointed out by Slater,[29] near atomic nuclei the crystalline potential in a solid is similar to that of a single atom, while in the region between nuclei (in the interstitial) the potential is rather smooth and weakly varying. Hence, one may introduce a set of basis functions, *augmented plane waves*, adapted to this general shape of the potential. First the crystal space is divided into nonoverlapping muffin-tin (MT) spheres centered at the atomic sites and the interstitial region in between. In the interstitial region (I) the APW $\phi^{\mathbf{k}}_{\mathbf{G}}(\mathbf{r})$ is simply the corresponding plane wave for given reciprocal lattice vector $\mathbf{G}$ and crystal momentum $\mathbf{k}$:

$$\phi^{\mathbf{k}}_{\mathbf{G}}(\mathbf{r}) = \frac{1}{\sqrt{V}}e^{i(\mathbf{k}+\mathbf{G})\mathbf{r}}, \quad \mathbf{r}\in I, \quad (15)$$

where V is the unit cell volume. This plane wave is augmented inside each of the MT spheres by a combination of the radial solutions of the Schrödinger equation in such a way that the resulting APW is continuous at the sphere boundary. The APW are then employed to expand the KS eigenstates $\psi^{\sigma}_{\mathbf{k}\nu}(\mathbf{r})$ for the full KS potential (without any shape approximation). In the original formulation of the APW method the radial solutions expanding a KS eigenstate inside MT spheres had to be evaluated at the corresponding eigenenergy leading to an energy-dependent basis set and, hence, to a nonlinear secular problem. In order to avoid this complication, linearized versions of the APW method have been proposed. There are two widely used schemes for the APW linearization. In the first, the linear APW (LAPW) method,[30] the plane wave is augmented within MT spheres by a combination of the radial solutions, evaluated at chosen linearization energies E_{1l}, and their energy derivatives. The resulting linear augmented plane wave then reads

$$\phi_{\mathbf{G}}^{\mathbf{k}}(\mathbf{r}) = \begin{cases} \frac{1}{\sqrt{V}} e^{i(\mathbf{k}+\mathbf{G})\mathbf{r}}, & \mathbf{r} \in I \\ \sum_{lm} [A_{lm}^{\alpha,\mathbf{k}+\mathbf{G}} u_l^{\alpha,\sigma}(r,E_{1l}^{\alpha}) + B_{lm}^{\alpha,\mathbf{k}+\mathbf{G}} \dot{u}_l^{\alpha,\sigma}(r,E_{1l}^{\alpha})] Y_m^l(\hat{r}), & \mathbf{r} \in R_{\mathrm{MT}}^{\alpha}, \end{cases} \tag{16}$$

where the index $\alpha = 1, \ldots, N_{\mathrm{at}}$ runs over all N_α atomic sites in the unit cell, the coefficients A_{lm} and B_{lm} are determined from the requirement for the linear APW to be continuous and differentiable at the sphere boundary, and r and $\hat{r}$ are the radial and angular parts of the position vector, respectively. The energy-independent basis set (16) leads to a linear secular problem, however, compared to the energy-dependent APW, a larger number of the LAPW in the basis set is generally required to attain the same accuracy. In order to decrease the requirement for the number of APW another linearization scheme, APW+lo (Ref. 31) has been proposed. The APW+lo basis set consists of the augmented plane waves evaluated at a fixed energy E_{1l}:

$$\phi_{\mathbf{G}}^{\mathbf{k}}(\mathbf{r}) = \begin{cases} \frac{1}{\sqrt{V}} e^{i(\mathbf{k}+\mathbf{G})\mathbf{r}}, & \mathbf{r} \in I \\ \sum_{lm} A_{lm}^{\alpha,\mathbf{k}+\mathbf{G}} u_l^{\alpha,\sigma}(r,E_{1l}^{\alpha}) Y_m^l(\hat{r}), & \mathbf{r} \in R_{\mathrm{MT}}^{\alpha}, \end{cases} \tag{17}$$

where the coefficient A_{lm} is determined from the requirement for $\phi_{\mathbf{G}}^{\mathbf{k}}(\mathbf{r})$ to be continuous at the sphere boundary. To increase the variational freedom of the APW+lo basis set the fixed-energy APW (17) are supplemented for the physically important orbitals (with $l \leq 3$) by the local orbitals (lo) that are not matched to any plane wave in the interstitial and are defined only within the muffin-tin spheres ($\mathbf{r} \in R_{\mathrm{MT}}^{\alpha}$),

$$\phi_{lm,\alpha}^{\mathrm{lo}}(\mathbf{r}) = [A_{lm}^{\alpha,\mathrm{lo}} u_l^{\alpha,\sigma}(r,E_{1l}^{\alpha}) + B_{lm}^{\alpha,\mathrm{lo}} \dot{u}_l^{\alpha,\sigma}(r,E_{1l}^{\alpha})] Y_m^l(\hat{r}), \tag{18}$$

with the coefficients A_{lm} and B_{lm} chosen from the requirement of zero value and slope for the local orbital at the sphere boundary.

Additional local orbitals (usually abbreviated with the capital letters as LO, $\phi_{lm,\alpha}^{\mathrm{LO}}$) can be introduced to account for semicore states. They have a similar form as Eq. (18) with the redefined $A_{lm}^{\alpha,\mathrm{LO}}$ and a second term with a coefficient $C_{lm}^{\alpha,\mathrm{LO}}$ and the radial function evaluated at a corresponding energy E_{2l}^{α} for the semicore band. The coefficient B_{lm} is set to 0 in the APW+lo framework.

Generally, in the full-potential augmented plane-wave method the LAPW, APW+lo, and LO types of orbitals can be employed simultaneously. The Kohn-Sham eigenstate is expanded in this mixed basis as

$$\psi_{k\nu}^{\sigma}(\mathbf{r}) = \sum_{i=1}^{N_b} c_{i\nu} \phi_i^{\sigma}(\mathbf{r}), \tag{19}$$

where N_b is the number of the orbitals in the basis set. The LDA+DMFT framework introduced in the present work can also be used in conjunction with any mixed APW+lo/LAPW/LO basis set.

3. Local orbitals and Wannier functions in the APW basis

Having defined the basis set we may now write down the expression for the Bloch eigenstate expanded in the general APW basis (19). For $\mathbf{r}$ in the interstitial region, it reads

$$\psi_{\mathbf{k}\nu}^{\sigma}(\mathbf{r}) = \frac{1}{\sqrt{V}} \sum_{\mathbf{G}}^{N_{\mathrm{PW}}} c_{\mathbf{G}}^{\nu,\sigma}(\mathbf{k}) e^{i(\mathbf{k}+\mathbf{G})\mathbf{r}}, \tag{20}$$

while for the region within the MT spheres $\mathbf{r} \in R_{\mathrm{MT}}^{\alpha}$ ($\alpha = 1, \ldots, N_{\mathrm{at}}$), we have

$$\begin{aligned} \psi_{\mathbf{k}\nu}^{\sigma}(\mathbf{r}) = & \sum_{\mathbf{G}}^{N_{\mathrm{PW}}} c_{\mathbf{G}}^{\nu,\sigma}(\mathbf{k}) \sum_{lm} A_{lm}^{\alpha,\mathbf{k}+\mathbf{G}} u_l^{\alpha,\sigma}(r,E_{1l}^{\alpha}) Y_m^l(\hat{r}) \\ & + \sum_{n_{\mathrm{lo}}=1}^{N_{\mathrm{lo}}} c_{\mathrm{lo}}^{\nu,\sigma} [A_{lm}^{\alpha,\mathrm{lo}} u_l^{\alpha,\sigma}(r,E_{1l}^{\alpha}) + B_{lm}^{\alpha,\mathrm{lo}} \dot{u}_l^{\alpha,\sigma}(r,E_{1l}^{\alpha})] Y_m^l(\hat{r}) \\ & + \sum_{n_{\mathrm{LO}}=1}^{N_{\mathrm{LO}}} c_{\mathrm{LO}}^{\nu,\sigma} [A_{lm}^{\alpha,\mathrm{LO}} u_l^{\alpha,\sigma}(r,E_{1l}^{\alpha}) \\ & + C_{lm}^{\alpha,\mathrm{LO}} u_l^{\alpha,\sigma}(r,E_{2l}^{\alpha})] Y_m^l(\hat{r}), \end{aligned} \tag{21}$$

where N_{PW} is the total number of plane waves considered in the interstitial which in turn is augmented inside each MT sphere, N_{lo} is the number of $\phi_{lm,\alpha}^{\mathrm{lo}}(\mathbf{r})$ orbitals of Eq. (18) and N_{LO} the corresponding number of auxiliary orbitals for semicore states $\phi_{lm,\alpha}^{\mathrm{LO}}(\mathbf{r})$.

In the framework of the APW method one has several choices for the "initial" correlated orbitals $|\chi_m^{\alpha,\sigma}\rangle$. Any suitable combination of the radial solution of the Schrödinger equation and its energy derivative for a given correlated shell $\{\alpha, l\}$ can be employed, for example, the lo orbital (18). In the present paper we simply chose the $|\chi_m^{\alpha,\sigma}\rangle$'s as the solutions of the Schrödinger equation within the MT sphere $|u_l^{\alpha,\sigma}(E_{1l}) Y_m^l\rangle$ at the corresponding linearization energy E_{1l}.

Inserting $|\chi_m^{\alpha,\sigma}\rangle = |u_l^{\alpha,\sigma}(E_{1l}) Y_m^l\rangle$ and expansion (21) of the Bloch eigenstate in terms of APWs into Eqs. (10) and (11), and making use of the orthonormality of the radial solutions and their energy derivatives,

$$\langle u_l^{\alpha,\sigma}(E_{1l}) Y_m^l | u_{l'}^{\alpha,\sigma}(E_{1l}) Y_{m'}^{l'} \rangle = \delta_{ll'mm'}, \tag{22}$$

$$\langle u_l^{\alpha,\sigma}(E_{1l}) Y_m^l | \dot{u}_{l'}^{\alpha,\sigma}(E_{1l}) Y_{m'}^{l'} \rangle = 0, \tag{23}$$

one obtains the following expression for the projection operator matrix element:

$$\tilde{P}^{\alpha,\sigma}_{m\nu}(\mathbf{k}) = \langle u^{\alpha,\sigma}_{l}(E_{1l}) Y^{l}_{m} | \psi^{\sigma}_{\mathbf{k}\nu} \rangle = A^{\nu,\alpha}_{lm}(\mathbf{k},\sigma) + \sum_{n_{\mathrm{LO}}=1}^{N_{\mathrm{LO}}} C^{\nu,\alpha}_{lm,\mathrm{LO}}(\mathbf{k},\sigma). \tag{24}$$

In this expression, the first term in the right-hand side of Eq. (24) is due to the contribution from the LAPW and/or APW+lo orbitals,

$$A^{\nu,\alpha}_{lm}(\mathbf{k},\sigma) = \sum_{\mathbf{G}}^{N_{\mathrm{PW}}} c^{\nu,\sigma}_{\mathbf{G}}(\mathbf{k}) A^{\alpha,\mathbf{k}+\mathbf{G}}_{lm} + \sum_{n_{\mathrm{lo}}=1}^{N_{\mathrm{lo}}} c^{\nu,\sigma}_{\mathrm{lo}} A^{\alpha,\mathrm{lo}}_{lm} + \sum_{n_{\mathrm{LO}}=1}^{N_{\mathrm{LO}}} c^{\nu,\sigma}_{\mathrm{LO}} A^{\alpha,\mathrm{LO}}_{lm}, \tag{25}$$

and the contribution due to the LO (semicore) orbitals that arises due to mutual nonorthogonality of the radial solutions of the Schrödinger equation for different energies

$$C^{\nu,\alpha}_{lm,\mathrm{LO}}(\mathbf{k},\sigma) = c^{\nu,\sigma}_{\mathrm{LO}} C^{\alpha,\mathrm{LO}}_{lm} \tilde{O}^{\alpha,\sigma}_{lm,l'm'}, \tag{26}$$

where $\tilde{O}^{\alpha,\sigma}_{lm,l'm'}$ is the corresponding overlap:

$$\tilde{O}^{\alpha,\sigma}_{lm,l'm'} = \langle u^{\alpha,\sigma}_{l}(E_{1l}) Y^{l}_{m} | u^{\alpha,\sigma}_{l'}(E_{l,\mathrm{LO}}) Y^{l'}_{m'} \rangle \neq 0. \tag{27}$$

Then we orthonormalize the obtained local orbitals to form a set of Wannier-type functions, Eq. (12). The corresponding projection operator matrix elements (24) are orthonormalized accordingly using Eq. (14).

B. Implementation and computational methods

1. FLAPW code

For the electronic structure calculation we use the full-potential APW+lo/LAPW code as implemented in the WIEN2K package.[1] We have built an interface that constructs the projectors to the correlated orbitals $[P^{\alpha,\sigma}_{m\nu}(\mathbf{k})]$ out of the eigenstates produced by the WIEN2K code, as described in Sec. II A 3. In order to obtain the local Green's function, the summation over momenta, Eq. (6), is done in the irreducible Brillouin zone (BZ) only, supplemented by a symmetrization procedure which is standard in electronic structure calculations,

$$\sum_{\mathbf{k}}^{\mathrm{BZ}} \mathbf{A}(\mathbf{k}) = \sum_{s=1}^{N_s} \sum_{\mathbf{k}}^{\mathrm{IBZ}} \mathcal{O}_s \mathbf{A}(\mathbf{k}) \mathcal{O}_s^{\dagger}, \tag{28}$$

where $\mathbf{A}(\mathbf{k})$ is any $\mathbf{k}$-dependent matrix, N_s the number of symmetry operations, and $\mathcal{O}_s$ the symmetrization matrices. Furthermore, we construct the local orbitals in the local coordinate system of the corresponding atom. This means that the equivalent atoms in the unit cell for which the DMFT should be applied, e.g., the two Fe atoms in the oxypnictides, are exactly the same and the impurity problem has to be solved only once. Afterward, the Green's function and self-energies are put back to the global coordinate system of the crystal in which the Bloch Green's function, Eq. (3), is formulated.

2. Continuous-time quantum Monte Carlo

For the solution of the impurity problem we use the strong-coupling version of the continuous-time quantum Monte Carlo (CTQMC) method.[27,28] It is based on a hybridization expansion and has proved to be a very efficient solver for quantum impurity models in the weak and strong correlation regime. It allows us to address room temperature ($\beta \equiv 1/kT \approx 40\ \mathrm{eV}^{-1}$) without problems. In our calculations, we used typically around 5×10^6 Monte Carlo sweeps and 1000 $\mathbf{k}$ points in the irreducible BZ. Since the CTQMC solver computes the Green's function on the imaginary-time axis, an analytic continuation is needed in order to obtain results on the real-frequency axis. Here, we choose to perform a continuation of the impurity self-energy using a stochastic version of the maximum entropy method[32] yielding real and imaginary parts of the retarded self-energy $\mathrm{Re}\,\Sigma(\omega+i0^+), \mathrm{Im}\,\Sigma(\omega+i0^+)$ which can be inserted into Eq. (3) in order to obtain the lattice spectral function and density of states.

3. Many-body interactions

The CTQMC strong-coupling algorithm can deal with the full rotationally invariant form of the interaction Hamiltonian.[28] However, most calculations presented in this paper will consider only the Ising terms of the Hund's coupling yielding the interaction Hamiltonian

$$H_{\mathrm{int}} = \frac{1}{2} \sum_{mm',\sigma} U^{\sigma\sigma}_{mm'} n_{m\sigma} n_{m'\sigma} + \frac{1}{2} \sum_{mm'} U^{\sigma\bar{\sigma}}_{mm'} (n_{m\uparrow} n_{m'\downarrow} + n_{m\downarrow} n_{m'\uparrow}), \tag{29}$$

with $U^{\sigma\sigma}_{mm'}$ and $U^{\sigma\bar{\sigma}}_{mm'}$ as the reduced interaction matrices for equal and opposite spins, respectively. This enables us to take advantage of a maximal amount of conserved quantum numbers and, hence, perform the CTQMC calculation without any truncation of the local basis. The effects of spin-flip and "pair-hopping" terms in the Hund's interaction are discussed in Appendix C.

In our approach, the interaction matrices are expressed in terms of the Slater integrals F^0, F^2, and F^4, where for d electrons these parameters are related to the Coulomb and Hund's coupling via $U=F^0$, $J=(F^2+F^4)/14$, and $F^2/F^4=0.625$.[33] Using standard techniques the four-index U matrix is calculated and the reduced interaction matrices are then given by $U^{\sigma\bar{\sigma}}_{mm'} = U_{mm'mm'}$ and $U^{\sigma\sigma}_{mm'} = U_{mm'mm'} - U_{mm'm'm}$. With the above definitions, the Coulomb parameters U and J are related to the matrices via

$$U = \frac{1}{N^2} \sum_{mm'}^{N} U^{\sigma\bar{\sigma}}_{mm'}, \tag{30}$$

$$J = U - \frac{1}{N(N-1)} \sum_{m\neq m'}^{N} U^{\sigma\sigma}_{mm'}. \tag{31}$$

As mentioned above, the LDA+DMFT scheme (as the LDA+U one) involves a double-counting correction $\Sigma^{\mathrm{dc}}_{mm'}$ in Eqs. (4) and (5). Indeed, on-site Coulomb interactions are

already treated on mean-field level in LDA. Several forms of the double-counting correction term have been proposed and investigated.[33–35] In this work we follow Ref. 33 and use the following double-counting correction:

$$\Sigma_{mm'}^{\sigma,\mathrm{dc}} = \delta_{mm'}\left[U\left(N_c - \frac{1}{2}\right) - J\left(N_c^{\sigma} - \frac{1}{2}\right)\right], \qquad (32)$$

where U is the average Coulomb interaction, J is the Hund's rule coupling, N_c^{σ} is the spin-resolved occupancy of the correlated orbitals, and $N_c = N_c^{\uparrow} + N_c^{\downarrow}$. We compared the results obtained with Eq. (32) also with the double-counting correction given in Ref. 36 which gave very similar results.

C. Choice of energy window, localization of Wannier functions, and screening

The Wannier functions defining the correlated subspace of orbitals for which a DMFT treatment is performed are constructed by truncating the expansion of the initial atomiclike local orbitals to a restricted energy window $\mathcal{W}$ as described above. The choice of this energy window is an important issue, which deserves further discussion. Indeed, it will determine the shape and the degree of localization of the resulting Wannier-type functions.

Let us consider first the case of a rather small energy window containing only those bands that have dominantly an orbital character which qualifies them as "correlated" (e.g., the Fe-3d orbitals in LaFeAsO or the V-3d-t_{2g} orbitals in $SrVO_3$). In that case, the dimension of the Kohn-Sham Hamiltonian used in Eq. (3) coincides with that of the correlated subspace $\mathcal{C}$ (i.e., with the number of orbitals involved in the effective impurity model, for a single correlated atom per cell). The Wannier-type functions are then quite extended in real space and resemble strongly the Wannier orbitals constructed within other schemes, such as the maximally localized Wannier construction of Ref. 20 or the Nth order muffin-tin basis set downfolded to that set of bands.[37–39] In such a situation, hybridization of the correlated orbitals with states that lie outside the energy window is neglected at the DMFT level. Some information about the hybridization, e.g., of the d states with ligand orbitals is of course taken into account through the leakage of the Wannier orbitals on neighboring ligand sites (see, e.g., Ref. 40).

In contrast, if a larger energy window is chosen, it will in general contain states treated as correlated as well as states on which no Hubbard interactions are imposed. In this case, the dimension of the Kohn-Sham Hamiltonian used in the LDA+DMFT calculation of the local Green's functions (3) and (6) exceeds the number of correlated orbitals involved in the effective impurity model. The Wannier functions are more localized in space and the information about the hybridization of the correlated orbitals with other states within this larger window is carried by the off-diagonal blocks of the Hamiltonian between correlated and uncorrelated states.

An instructive case occurs when the correlated bands are well separated from the uncorrelated bands at all **k** points, but the bands overlap in energy. This situation is realized for instance for the t_{2g} bands in $SrVO_3$ that extend into the energy region of the e_g bands. In order to strictly pick the three correlated t_{2g} bands at each **k** point, one would in that case have to introduce a **k**-dependent energy window. For a **k**-independent energy window, one will in general have more than three bands at some **k** points corresponding to some e_g contribution in the chosen window. This can then be expected to result in slightly more localized orbitals. An example is given in Appendix A.

D. Local Coulomb interactions, screening, and constrained RPA calculations

The choice of the energy window influences the value of the interaction parameters $U_{mm'm''m'''}$ in a crucial manner, which can be traced back to two main reasons. First, the interaction parameters are related to matrix elements of a screened interaction between the chosen Wannier functions. The more bands are included in their construction, the more localized they become and, hence, the matrix elements increase. Second, screening effects themselves affect the value of U. The more states are excluded from the screening process, the larger U becomes. In what follows we distinguish carefully between these two effects.

In the present work, we apply the present LDA+DMFT implementation to one of the new high-T_c superconductors, LaFeAsO. For constructing the Wannier functions, we focus on an energy window that contains the ten bands around the Fermi level with dominantly Fe-3d character and also the bands coming from the p bands of O and As, which are mainly located in the energy region $[-6,-2]$ eV, resulting in a "dpp Hamiltonian." In addition, we performed calculations also for a smaller energy window containing only the Fe-3d bands yielding a "d Hamiltonian," as well as for a very large window including around 60 Bloch bands.

The values of the Coulomb interactions U and J are calculated from the constrained random-phase approximation (cRPA),[41,42] using the recently developed scheme for entangled band structures.[43] cRPA calculations for LaFeAsO have been performed before in Refs. 44 and 45. In Ref. 45 the screened Coulomb parameters are obtained for three different situations: (i) by constructing Wannier functions from an energy window comprising the Fe-d bands only and screening calculated excluding the Fe-d channels only, (ii) by considering a larger window which also includes the As and O-p states, so that the screening processes, for instance, from the As-p states to the Fe-d ones are also excluded, (iii) and finally, a hybrid situation (dubbed "d-dpp" in Ref. 45), in which the Wannier functions are calculated from an energy window including Fe-d, O-p, and As-p, but only the Fe-d states are excluded from the screening. In other words, the screening is calculated as in (i) and the Wannier functions as in (ii). As discussed in Ref. 45, this third option should be appropriate in a situation in which a full dpp Hamiltonian is used but Hubbard interactions are only applied to the d states.

Here, we follow the same approach as in the d-dpp case of Ref. 45, but using the new disentanglement scheme of Ref. 43. First, a partially screened Coulomb interaction W_r is constructed as follows: Wannier functions for the Fe-d states are calculated and a basis for the complementary subspace

(containing in particular the ligands, but also higher lying f states) is constructed. Based on the interpolating d-band structure, the P_d polarization is computed and the partially screened Coulomb interaction W_r is obtained by screening the bare Coulomb interaction by all RPA screening processes *except* P_d. Finally, according to the cRPA procedure the Hubbard U matrix is composed of the matrix elements of W_r in the basis of *dpp*-Wannier functions. As argued in Ref. 45 this procedure is suitable for calculations that deal with the full *dpp* Hamiltonian in the many-body calculations while explicitly retaining Coulomb interactions on the d submanifold only. In particular, we stress that to the extent that our projection method produces Wannier functions for the *dpp* window, the Hubbard U parameters are expressed in the same basis as the impurity quantities.

It is important to note that we keep the screening channels in cRPA, i.e., P_d, unchanged when the energy window in our calculation is varied. Thus, the different energy windows affect only the localization of the Wannier functions, but not the screening process of the bare Coulomb interaction, and therefore the effective interactions are increasing with increasing energy window. Keeping the screening channels fixed is fully consistent with the fact that correlations are only included for the d electrons but not for the ligand states.

For our purposes, we calculate the average Coulomb interaction U and Hund's parameter J from the matrices calculated by cRPA. With this U and J, the interaction matrices in the spherical symmetric approximation used in our calculation are obtained as discussed above. As we will discuss in more detail below, the comparison of the resulting $U^{\sigma\sigma}_{mm'}$ and $U^{\sigma\bar{\sigma}}_{mm'}$ with the cRPA matrices shows that for the *dpp* Hamiltonian, the approximation using atomic values for the ratios of Slater integrals F^k is well justified, whereas for the d Hamiltonian the cRPA matrices show strong orbital anisotropies.

III. RESULTS FOR THE IRON OXYPNICTIDE LaFeAsO

A. Construction of the *dpp* Hamiltonian

Let us start the discussion of correlation effects in LaFeAsO with our results for the *dpp* Hamiltonian, for which Wannier functions are constructed from the energy window $\mathcal{W}=[-5.5,2.5]$ eV. These Wannier functions are quite well localized. The corresponding Kohn-Sham Hamiltonian contains 22 Bloch bands corresponding to the ten Fe-3d bands, the six As-p bands, and the six O-p bands.

The local many-body interactions corresponding to this choice of Wannier functions are obtained from cRPA, as described in the previous section. They read as

$$U^{\sigma\sigma}_{mm'}|_{\mathrm{cRPA}} = \begin{pmatrix} 0.00 & 1.61 & 1.55 & 2.26 & 2.26 \\ 1.61 & 0.00 & 2.50 & 1.82 & 1.82 \\ 1.55 & 2.50 & 0.00 & 1.70 & 1.70 \\ 2.26 & 1.82 & 1.70 & 0.00 & 1.74 \\ 2.26 & 1.82 & 1.70 & 1.74 & 0.00 \end{pmatrix},$$

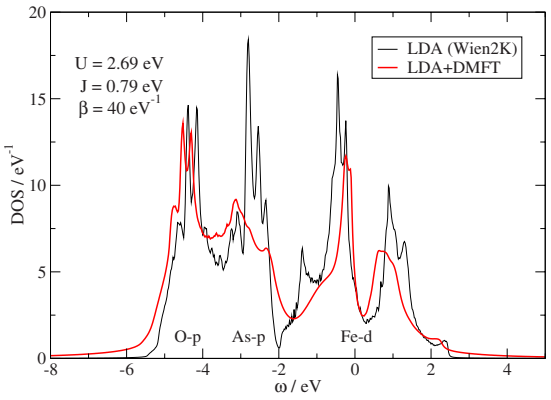

FIG. 1. (Color online) Total DOS for LaOFeAs, *dpp* Hamiltonian. Black line: LDA DOS. Red line: LDA+DMFT DOS.

$$U^{\sigma\bar{\sigma}}_{mm'}|_{\mathrm{cRPA}} = \begin{pmatrix} 3.77 & 2.35 & 2.21 & 2.71 & 2.71 \\ 2.35 & 3.94 & 2.87 & 2.44 & 2.44 \\ 2.21 & 2.87 & 3.31 & 2.29 & 2.29 \\ 2.71 & 2.44 & 2.29 & 3.48 & 2.29 \\ 2.71 & 2.44 & 2.29 & 2.29 & 3.48 \end{pmatrix}.$$

The ordering of orbitals in those matrices is d_{z^2}, $d_{x^2-y^2}$, d_{xy}, d_{xz}, and d_{yz}.

According to the conventions of the formulae Eqs. (30) and (31), these matrices correspond to the values $U=2.69$ eV and $J=0.79$ eV. Using these values of U and J, we construct the spherically symmetric interaction matrices,

$$U^{\sigma\sigma}_{mm'} = \begin{pmatrix} 0.00 & 1.49 & 1.49 & 2.30 & 2.30 \\ 1.49 & 0.00 & 2.57 & 1.76 & 1.76 \\ 1.49 & 2.57 & 0.00 & 1.76 & 1.76 \\ 2.30 & 1.76 & 1.76 & 0.00 & 1.76 \\ 2.30 & 1.76 & 1.76 & 1.76 & 0.00 \end{pmatrix},$$

$$U^{\sigma\bar{\sigma}}_{mm'} = \begin{pmatrix} 3.59 & 2.19 & 2.19 & 2.73 & 2.73 \\ 2.19 & 3.59 & 2.91 & 2.37 & 2.37 \\ 2.19 & 2.91 & 3.59 & 2.37 & 2.37 \\ 2.73 & 2.37 & 2.37 & 3.59 & 2.37 \\ 2.73 & 2.37 & 2.37 & 2.37 & 3.59 \end{pmatrix}.$$

It is obvious that the approximation of the cRPA matrices by using spherical symmetrization is well justified in this case, with the largest absolute deviation being $\Delta U \approx 0.35$ eV, corresponding to a relative error of around 0.09. The reason for this good agreement is that in the present case the Wannier functions are already very close to atomiclike orbitals. We also checked that cRPA yields a significantly larger value of U for iron-oxide (FeO), as expected physically.

B. LDA+DMFT results (*dpp* Hamiltonian)

We carried out LDA+DMFT calculations for the *dpp* Hamiltonian using the above matrices at an inverse temperature $\beta=40$ eV^{-1} (room temperature $T=300$ K), using the experimental crystal structure of LaFeAsO. In Fig. 1 we dis-

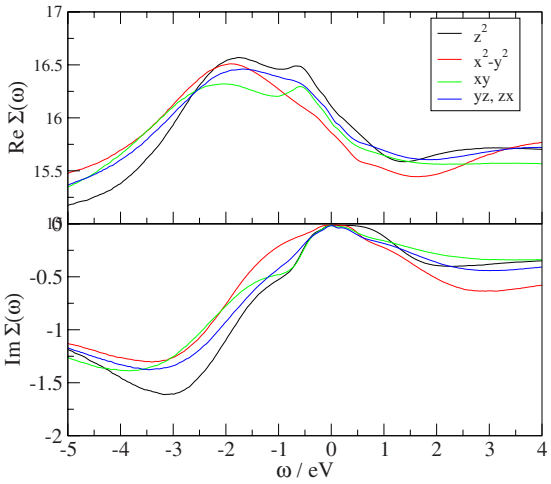

FIG. 2. (Color online) Real (top) and imaginary (bottom) parts of the orbital-dependent self-energy in the *dpp* Hamiltonian for $U=2.69$ and $J=0.79$.

play the resulting total densities of states (DOS) together with the corresponding LDA DOS. The total densities of states were computed from the lattice Green's function, Eq. (3), traced over all $\nu \in \mathcal{W}$ and integrated over BZ. In order to obtain the corresponding LDA densities of states $\Sigma^{\sigma}_{\nu\nu'}(\mathbf{k}, i\omega_n)$ in Eq. (3) was set to zero.

One sees in Fig. 1 that the LDA+DMFT DOS near the Fermi level displays characteristic features of a metal in an intermediate range of correlations. Both occupied and empty states are shifted toward the Fermi level due to the Fermi-liquid renormalizations. No high-energy features that would correspond to lower or upper Hubbard bands are present in the LDA+DMFT electronic structure. The Fermi-liquid behavior is clear from the self-energy on the real-frequency axis, which we plot in Fig. 2 for the *dpp* Hamiltonian. Although it shows a quite rich structure as a function of energy, the real part displays clear linear behavior at low frequency. The imaginary part is small around $\omega=0$ and has a quadratic frequency dependence at low frequency. It does increase to rather large values at higher frequencies, however, especially for occupied states. Hence, our results are in general agreement with the previous calculations of Anisimov *et al.*[4] and with the experimental photoemission spectra (PES) (Ref. 46) and x-ray absorption[47] spectra of LaFeAsO, which report a moderately correlated system with mass renormalization around 1.8–2.0.

In order to analyze the strength of correlations for different Fe $3d$ orbitals we calculated the corresponding quasiparticle residues $Z_m=\{1-\mathrm{Im}[\frac{d\Sigma_{mm}(\omega)}{d\omega}|_{\omega\to 0}]\}^{-1}$ from the self-energy Eq. (5) on the Matsubara grid (hence, avoiding all uncertainties related to the analytical continuation). The values are 0.609, 0.663, 0.609, and 0.596 for the d_{z^2}, $d_{x^2-y^2}$, d_{xy}, and degenerate d_{xz}/d_{yz} orbitals, respectively. In this *dpp* energy window the Wannier functions become quite localized and their spread is expected to be isotropic. Indeed, within the *dpp* Hamiltonian the difference in Z_m between the orbitals is rather small. The resulting value for the average mass renormalization (between 1.5 and 1.7) is in reasonable agreement with the experimental estimate of 1.8 extracted in Ref. 46 from experimental PES. The smaller mass renormalization found in our calculation compared to the experimental value can be attributed to the single-site approximation of DMFT. Spatial spin fluctuations, which are completely neglected in this approach, can eventually increase the effective mass of the quasiparticles.

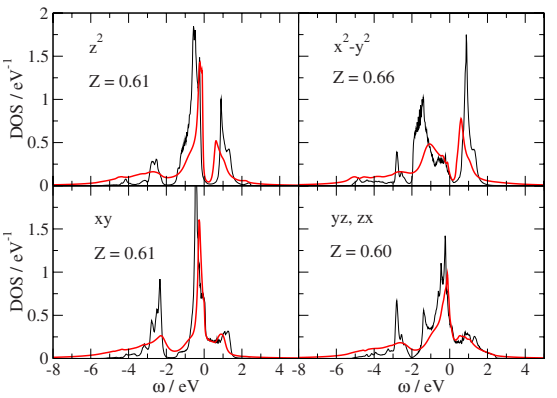

FIG. 3. (Color online) DOS of Fe orbitals in LaOFeAs, *dpp* Hamiltonian. Color coding as in Fig. 1.

The partial densities of states for all Fe $3d$ orbitals computed within the *dpp* model are displayed in Fig. 3. The partial LDA+DMFT DOS for the x^2-y^2 and yz, xz orbitals are shifted upward relative to the xy. Indeed, we found that the crystal-field (CF) splitting between the Fe $3d$ orbitals is somewhat affected by correlations. The splitting between the lowest xy and highest z^2 orbitals remains unchanged (≈ 0.3 eV), while the x^2-y^2 and yz, xz CF levels are shifted upward by 0.15 and 0.08 eV relative to their positions in LDA. In LDA+DMFT they are located at 0.25 and 0.18 eV, respectively, above the xy orbital.

It is also instructive to look at the momentum-resolved spectral function $A(\mathbf{k}, \omega)$ of the crystal. It is obtained from the lattice Green's function, Eq. (3), using the real-frequency self-energy and tracing over the orbital degrees of freedom. The result for the *dpp* model is shown in Fig. 4 for an energy range including Fe-*d*, As-*p*, and O-*p* states. In agreement with the Fermi-liquid picture of moderately correlated quasiparticles discussed above, one can see well-defined excita-

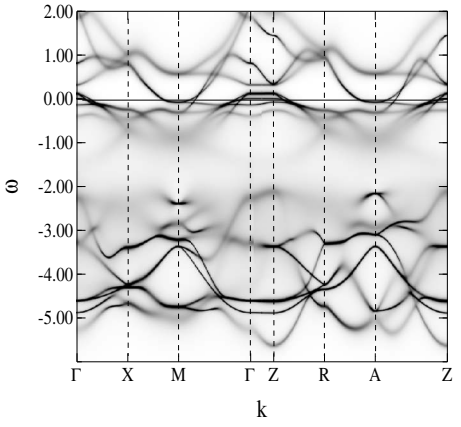

FIG. 4. Momentum-resolved spectral function of LaOFeAs, *dpp* Hamiltonian. Dark areas mark large spectral weight.

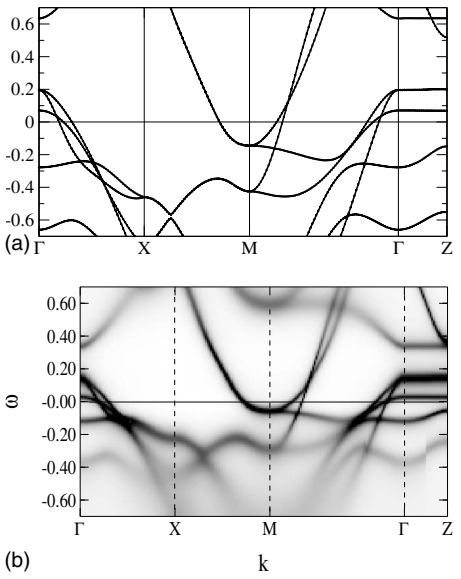

FIG. 5. Comparison of the momentum-resolved spectral function of LaOFeAs at low energies. Upper panel: LDA. Lower panel: LDA+DMFT *dpp* Hamiltonian.

tions around the Fermi level, which get more diffuse at higher binding energies. The bands above the Fermi level are less affected since the self-energies are quite asymmetric and smaller for positive frequencies; see Fig. 2. Additionally, it is easy to see that the As-*p* states, dominantly in the energy range $[-3.5,-2]$ eV, hybridize stronger with the Fe-*d* states and get, thus, affected by correlations. This effect is almost absent for the O-*p* states since they hybridize much less with Fe-*d*.

In Fig. 5 we show a comparison between the LDA band structure and the LDA+DMFT **k**-resolved electronic structure in a low-energy range around the Fermi level. This again reveals the coherent quasiparticles at the Fermi level, as well as more diffuse bands at higher energies. The crossover between long-lived quasiparticles and more diffuse states with a shorter lifetime is around −0.4 eV, in qualitative agreement with existing ARPES data.[48] A point to mention here is the effect of the CF splitting on the band structure. For example, a difference between the LDA and DMFT results can be seen for the excitation with predominantly *xy* character. In LDA it forms a hole pocket with an excitation energy of +0.08 eV at the Γ point. Due to correlations, however, this band is shifted down significantly to the Fermi level and the third hole pocket stemming from the d_{xy} orbital could eventually vanish upon electron doping.

One has to keep in mind that a direct comparison to experimental data is difficult for this compound, since (i) the experiments were done at low temperatures in the SDW phase, whereas our calculations are done at room temperature using the tetragonal crystal structure, and (ii) ARPES experiments on the 1111 family of pnictide superconductors are difficult to perform because of difficulties with single-crystal synthesis. Nevertheless, on a qualitative level, there is a satisfactory agreement between LDA+DMFT and experiments.

We also studied the dependence of the results on the values of the interaction parameters *U* and *J*. The resulting quasiparticle renormalizations Z_m are listed in Table I. Comparing the first two rows, one can see that a smaller value of *J* decreases the degree of correlations. The third line corresponds to values similar to the ones used in Ref. 4 giving very similar results. We also increased *U* to the (unphysically) large value of $U=5.0$ eV and the system still displays metallic behavior, although more correlated. Hence, our calculations strongly suggest that LaFeAsO is not close to a Mott metal-insulator transition.

TABLE I. Quasiparticle weights for different interaction parameters with Wannier orbitals constructed from $\mathcal{W}=[-5.5,2.5]$ eV (*dpp* Hamiltonian). The values in boldface correspond to the interaction parameters obtained from cRPA.

Interactions	z^2	x^2-y^2	xy	yz, zx
U=2.69, J=0.79	**0.61**	**0.66**	**0.61**	**0.60**
$U=2.69$, $J=0.60$	0.72	0.76	0.73	0.71
$U=3.70$, $J=0.80$	0.52	0.57	0.53	0.52
$U=5.00$, $J=0.80$	0.41	0.45	0.43	0.42

In order to check the robustness of our results, we also investigated the effect of increasing even further the spatial localization of the Wannier functions corresponding to a very large energy window $\mathcal{W}=[-5.5,13.6]$ eV. We did several calculations for different parameter sets and the resulting quasiparticle renormalizations Z_m of all these calculations are listed in Table II. For this case, no cRPA calculations for the interaction matrices were performed, but it is expected that *U* and *J* will slightly increase with more localized Wannier orbitals. In that sense, the first row of Table II corresponds to interaction parameters that could be realized for these Wannier functions. It is very satisfying to see the calculations gave almost identical quasiparticle renormalizations. Also the dependence on *U* and *J* is very similar to the one we found for the *dpp* Hamiltonian. In that sense we consider our calculations to be converged in terms of the number of Bloch bands that are included for the construction of the Wannier functions and the local Hamiltonian.

C. Remarks on calculations using the *d* Hamiltonian and extended Wannier functions

In this section, we address the LDA+DMFT calculations performed with the so-called *d* Hamiltonian, where only the ten Fe-*d* bands around the Fermi level are used for the construction of the Wannier orbitals. In doing so, we shall shed light on the discussion which has appeared in the literature[2–6]

TABLE II. Quasiparticle weights for different interaction parameters with the Wannier orbitals constructed for a very large window $\mathcal{W}=[-5.5,13.6]$ eV.

Interactions	z^2	x^2-y^2	xy	yz, zx
$U=3.00$, $J=0.80$	0.62	0.66	0.58	0.58
$U=3.00$, $J=0.60$	0.74	0.77	0.72	0.72
$U=3.70$, $J=0.80$	0.58	0.61	0.52	0.56

regarding the results of LDA+DMFT calculations by different authors and the degree of correlations of the 1111 family of pnictide superconductors.

1. Wannier functions and interaction matrices

The first thing to note is that the Wannier functions constructed from a small energy window encompassing only the Fe-*d* bands are quite extended and very anisotropic, as discussed in details in Ref. 40. This is directly reflected in the interaction matrices calculated by cRPA in this restricted energy window:

$$U^{\sigma\sigma}_{mm'}|_{\mathrm{cRPA}} = \begin{pmatrix} 0.00 & 1.41 & 1.26 & 1.87 & 1.87 \\ 1.41 & 0.00 & 1.91 & 1.54 & 1.54 \\ 1.26 & 1.91 & 0.00 & 1.33 & 1.33 \\ 1.87 & 1.54 & 1.33 & 0.00 & 1.44 \\ 1.87 & 1.54 & 1.33 & 1.44 & 0.00 \end{pmatrix},$$

$$U^{\sigma\bar{\sigma}}_{mm'}|_{\mathrm{cRPA}} = \begin{pmatrix} 3.17 & 2.02 & 1.72 & 2.22 & 2.22 \\ 2.02 & 3.36 & 2.16 & 2.04 & 2.04 \\ 1.72 & 2.16 & 2.17 & 1.73 & 1.73 \\ 2.22 & 2.04 & 1.73 & 2.73 & 1.84 \\ 2.22 & 2.04 & 1.73 & 1.84 & 2.73 \end{pmatrix},$$

which display a strong orbital dependence. For instance, the intraorbital (Hubbard) interaction spans from 2.17 to 3.36 eV. The interaction matrices in the spherical symmetric approximation using the averages $U=2.14$ and $J=0.59$ are

$$U^{\sigma\sigma}_{mm'} = \begin{pmatrix} 0.00 & 1.25 & 1.25 & 1.85 & 1.85 \\ 1.25 & 0.00 & 2.06 & 1.45 & 1.45 \\ 1.25 & 2.06 & 0.00 & 1.45 & 1.45 \\ 1.85 & 1.45 & 1.45 & 0.00 & 1.45 \\ 1.85 & 1.45 & 1.45 & 1.45 & 0.00 \end{pmatrix},$$

$$U^{\sigma\bar{\sigma}}_{mm'} = \begin{pmatrix} 2.82 & 1.77 & 1.77 & 2.18 & 2.18 \\ 1.77 & 2.82 & 2.31 & 1.91 & 1.91 \\ 1.77 & 2.31 & 2.82 & 1.91 & 1.91 \\ 2.18 & 1.91 & 1.91 & 2.82 & 1.91 \\ 2.18 & 1.91 & 1.91 & 1.91 & 2.82 \end{pmatrix}.$$

The largest deviation in this case is $\Delta U=0.65$ eV corresponding to a relative error of about 0.26. This shows clearly that the spherical approximation is highly questionable when using only the *d* bands for the Wannier construction. Of course, the full anisotropic interaction matrices can in principle be used in the LDA+DMFT calculation, but this raises the very delicate issue of a reliable *orbital-dependent* double-counting correction.

Another consequence of using delocalized Wannier functions is that they lead to significant nonlocal interactions V_{dd}, which we found to be (from cRPA) of order $0.23U$ to $0.32U$. These interactions are completely neglected in the single-site local DMFT approach suggesting the need for a cluster extension in that case. For these various reasons, we have reservations against using a *d*-only Hamiltonian with extended Wannier functions for DMFT calculations on LaFeAsO, as also previously emphasized in Ref. 40.

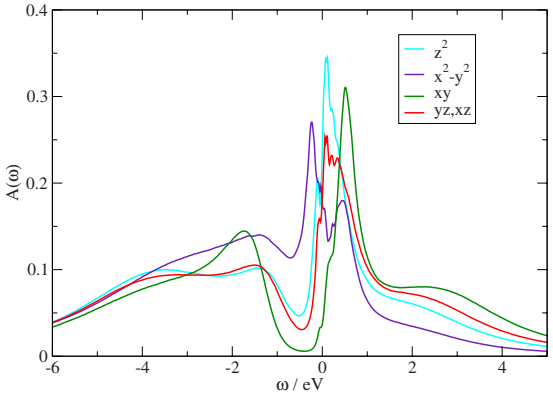

FIG. 6. (Color online) Impurity spectral function within the *d* Hamiltonian using interaction parameters $U=4.0$ eV and $J=0.7$ eV as have been used in Ref. 2. For those values a very correlated metal is obtained.

2. Consistency with previous calculations

Nevertheless, in order to clarify apparent discrepancies between previously published LDA+DMFT results,[2–6] we performed calculations within the *d* Hamiltonian for several interaction parameters reported in the literature. For the values $U=4.0$ eV and $J=0.7$ eV used in Ref. 2, we do confirm that the results then display very strong correlations with quasiparticle renormalizations ranging from $Z=0.11$ (xy orbital) to $Z=0.34$ (x^2-y^2 orbital). One may note that within the *d* model there is a substantial orbital dependence of Z_m, with a stronger renormalization predicted for the xy, yz, and zx orbitals. This is a clear consequence of the Wannier functions being much more delocalized and anisotropic.

The scattering rate at this inverse temperature of $\beta=40$ eV^{-1} is quite sizable [$\mathrm{Im}\,\Sigma(\omega^+=0)\approx -0.4,\ldots,-0.6$, depending on the orbital] showing that the system is on the verge of a coherence-incoherence crossover and a bad metal. The impurity spectral function is plotted in Fig. 6. It resembles very much the one shown in Fig. 3 of Ref. 2 showing clear signatures of lower and upper Hubbard bands. There are, though, some discrepancies with the total weight and the positions of the Hubbard bands, but given the differences in the calculation (underlying electronic structure method, temperature, interaction vertex which here is only density-density), this agreement with Ref. 2 is quite satisfactory.

Furthermore, using the parameters $U=0.8$ eV and $J=0.5$ eV from Ref. 4, we find renormalizations in the range $Z\approx 0.7-0.8$. This is somewhat smaller than reported in Ref. 4, although not in drastic disagreement.

Finally, we investigated the dependence on the Hund's rule coupling of calculations performed with the *d*-only Hamiltonian. Decreasing J to the much lower value $J=0.2$ eV but keeping $U=4$ eV, we find the system to be much less correlated (Z between 0.63 and 0.73). We thus confirm, for those calculations, the great sensitivity to the

Hund's coupling reported in Ref. 3. We note, however, that although reducing J does make the system somewhat less correlated in this case too, this sensitivity is much weaker when calculations are performed with the full *dpp* Hamiltonian as reported above.

3. Origin of the sensitivity to the Hund's coupling: Level crossings

In order to understand the origin of the remarkable sensitivity of the correlation strength to the value of J observed with the d Hamiltonian we have studied the evolution of the ground state of the Fe $3d$ atomic shell as function of J. We obtained the $3d$ level positions corresponding to two different choices of the energy window: the "small" one corresponding to the d Hamiltonian and comprising ten Fe $3d$ bands and the very large one comprising all As $4p$, O $2p$, and Fe $3d$ bands as well as all unoccupied bands up to 13 eV above E_F. The noninteracting level positions $\epsilon_{mm'}^{\alpha,\sigma}$ are then obtained as

$$\epsilon_{mm'}^{\alpha,\sigma} = \sum_{\mathbf{k},\nu\in\mathcal{W}} P_{m\nu}^{\alpha,\sigma} \epsilon_{\mathbf{k}\nu}^{\sigma} P_{\nu m'}^{\alpha,\sigma*} - \tilde{\Sigma}_{mm'}^{\sigma,\mathrm{dc}}, \tag{33}$$

where the double-counting term $\tilde{\Sigma}_{mm'}^{\sigma,\mathrm{dc}}$ is calculated in accordance with Eq. (32) but with the "atomic" occupancy $N=6$ of the Fe $3d$ shell. We used the same values of $U=2.14$ and 2.69 eV for the "small" and "very large" window choices, respectively, while the value of J was varied from 0.1 to 0.5 eV. With $\epsilon_{mm'}^{\alpha,\sigma}$ corresponding to the d Hamiltonian we observed a level crossing at $J\approx 0.2$ eV with the atomic ground state changing from the one with spin moment $S=1$ to the one with $S=2$. In the case of the very large window the ground state always corresponds to $S=2$ and the splitting between the ground state and first excited level is constant. It is obvious that a drastically different behavior of those two "atomic" models is related to the corresponding level positions $\epsilon_{mm'}$, which are computed using different choices for the Wannier orbitals. The observed change in the Fe $3d$ atomic ground state, induced by increasing J, hints on a possible strong dependence of correlation strength on the Hund's rule coupling for LaFeAsO, which is indeed observed in our LDA+DMFT calculations with the d Hamiltonian. However, this sensitivity stems from a particular choice of delocalized and anisotropic Wannier functions and is much less pronounced when the energy window for the Wannier function construction is increased.

The bottom line of this investigation is that all previously published calculations seem to be technically correct. However, as discussed above, one introduces several severe approximations when dealing with the d Hamiltonian only, and the justification of these approximations (restriction to local interactions, single-site DMFT, etc.) is questionable. This is especially true in this compound due to the strong covalency between iron and arsenic states.

IV. CONCLUSION AND PROSPECTS

In the first part of this work, we present an implementation of LDA+DMFT in the framework of the full-potential linearized augmented plane-wave method. We formulate the DMFT local impurity problem in the basis of Wannier orbitals, while the full lattice Green's function is written in the basis of Bloch eigenstates of the Kohn-Sham problem. In order to construct the Wannier orbitals for a given correlated shell we choose a set of local orbitals, which are then expanded onto the KS eigenstates lying within a certain energy window. In practice, we employ the radial solutions of the Schrödinger equation for a given shell evaluated at the corresponding linearization energy as local orbitals. By orthonormalizing the obtained set of basis functions we construct a set of true Wannier orbitals as well as projector operator matrices relating the Bloch and Wannier basis sets. We derive explicit formulas for the projected operator matrices in a general FLAPW framework, which may include different types of augmented plane waves, lo and LO orbitals. Our implementation is benchmarked using the test case of $SrVO_3$ for which we have obtained spectral and electronic properties in very good agreement with results of previous LDA+DMFT calculations.

In the second part of this paper we apply this LDA+DMFT technique to LaFeAsO in order to assess the degree of electronic correlations in this compound and clarify the ongoing controversy about this issue in the literature. We solved the DMFT quantum impurity problem using a continuous-time quantum Monte Carlo approach. The Wannier functions are constructed using an energy window comprising Fe $3d$, As $4p$, and O $2p$. The resulting Wannier orbitals are rather well localized and isotropic. We take the average values of $U=2.69$ eV and $J=0.79$ from constrained RPA calculations, where the Wannier functions and screening channels are consistent with our setting of the LDA+DMFT scheme. We have checked the robustness of these results by increasing the size of the energy window, which resulted in a very similar physical picture.

Our LDA+DMFT results indicate that LaFeAsO is a moderately correlated metal with an average value for the mass renormalization of the Fe $3d$ bands about 1.6. This value is in reasonable agreement with estimates from photoemission experiments.

We also consider a smaller energy window that includes Fe-d states only. The resulting Wannier functions in this case are quite extended leading to anisotropic and nonlocal Coulomb interactions. We take different values for U and J including the ones used in previous theoretical LDA+DMFT approaches. We demonstrate that different physical pictures ranging from a strongly correlated compound on the verge of the metal-insulator transition to a moderately to weakly correlated one can emerge depending, in particular, on the choice of the Hund's rule coupling J as observed in Ref. 3. However, there are conceptual difficulties when constructing a local Hamiltonian from rather delocalized Wannier orbitals. The interactions are very anisotropic and orbital dependent, and nonlocal interactions could also become important.

In summary, we demonstrate that the discrepancies in the results of several recent theoretical works employing the LDA+DMFT approach stem from two main causes: (i) the choice of parameters of the local Coulomb interaction on the Fe $3d$ shell and (ii) the degree of localization of the Wannier orbitals chosen to represent the Fe $3d$ states to which many-

body terms are applied. Regarding the first point, the calculated interaction parameters employed in the present work are significantly smaller than the values hypothesized in Refs. 2 and 3. Regarding the second point, we provide strong evidence that the DMFT approximation is more accurate and more straightforward to implement when well-localized orbitals are constructed from a large energy window encompassing Fe-3*d*, As-4*p*, and O-2*p*. This issue has fundamental implications for many-body calculations, such as DMFT, in a realistic setting.

ACKNOWLEDGMENTS

We are grateful to Vladimir Anisimov, Ryotaro Arita, Gabriel Kotliar, Igor Mazin, Frank Lechermann, Alexander Lichtenstein and, especially, Kristjan Haule for useful discussions and correspondence. M.A. is grateful to F. Assaad for enlightening discussions on the stochastic maximum entropy method. We acknowledge the support of the Agence Nationale de la Recherche (under project CORRELMAT), and of GENCI and IDRIS (under Project No. 091393) for supercomputer time. M.A. acknowledges financial support from the Austrian Science Fund (FWF) under Grant No. J2760-N16.

APPENDIX A: BENCHMARK—$SrVO_3$

For benchmarking purposes, we present in this appendix LDA+DMFT results for an oxide that has become a classical test compound for correlated electronic structure calculations, namely, the cubic perovskite $SrVO_3$. As a paramagnetic correlated metal with intermediate electron-electron interactions, it is in a regime that is neither well described by pure LDA calculations nor by approaches such as LDA+U that are geared at ordered insulating materials. From the experimental side, $SrVO_3$ has been characterized by different techniques (angle-resolved and angle-integrated photoemission spectroscopy, optics, transport, thermodynamical measurements, etc.).[17,23,49–57]

LDA+DMFT calculations have been performed both for an effective low-energy model that comprises the three degenerate bands of mainly t_{2g} character that are located around the Fermi energy—taking advantage of the cubic crystal field that singles out this group of bands—and for a bigger energy window comprising also the oxygen *p* states.[13,17,19,22,23,25,26,55,56]

In the low-energy effective t_{2g} model a quasiparticle renormalization of $Z\sim 0.6$, compatible with experiments, is obtained for *U* values around 4 eV. The remaining spectral weight is shifted toward lower and upper Hubbard bands. The lower Hubbard band located around −1.5 eV binding energy has indeed been observed in photoemission; the high-energy satellite of the t_{2g} model is located around 2.5 eV.[58]

Concerning calculations taking into account also the ligand states, it should be noted that possible LDA errors on the separation of *p* and *d* states are not corrected by DMFT, since only the *d* states are treated as correlated.

In the present work, we use $SrVO_3$ as a benchmark for our projector orbitals implementation of LDA+DMFT, with

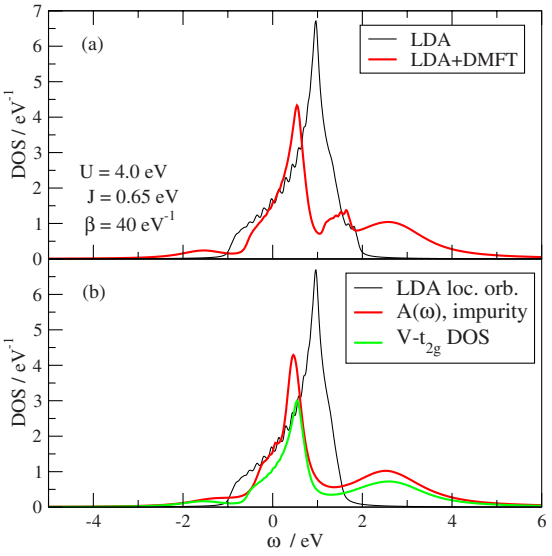

FIG. 7. (Color online) DOS for $SrVO_3$, *d*-only model (small energy window). Top panel (a): Total DOS of LDA (black) and LDA+DMFT (red). Bottom panel (b): LDA local orbitals (black), impurity spectral function $A(\omega)$ (red), and vanadium t_{2g} partial DOS (green). Coulomb parameters for these calculations are given as inset.

results very similar to previous theoretical studies. We performed two kinds of calculations: (i) we used as an energy window the range from −1.35 to 1.90 eV which comprises the t_{2g} bands, and—at some *k* points—one or both of the e_g bands. This is closest in spirit to a t_{2g} model within a Wannier function formalism, though not exactly the same due to the inclusion of some e_g contribution. To recover a Wannier prescription one would in fact have to choose a *k*-dependent window, such as to include exactly three bands *at each k* point, corresponding to the threefold degenerate manifold of dominantly t_{2g} bands. (ii) We used an energy window of −8.10 to 1.90 eV spanning both the bands used in (i) and the oxygen *p* dominated bands located between −8 and −2 eV.

Please note that, in order to be consistent with existing literature, we use a different parametrization of the interaction matrix compared to Sec. III. Here we define *U* to be the onsite intraorbital Coulomb interaction, $U-2J$ to be the interorbital interaction for electrons with opposite spin, and $U-3J$ the interorbital interaction between electrons with equal spin.

The results for the first case are shown in Fig. 7. The upper panel, Fig. 7(a), displays the total spectral function of the thus defined model within LDA and LDA+DMFT. Our results recover previously published results with a quasiparticle renormalization of around $Z=0.60$ for values $U=4.0$ eV and $J=0.65$ eV. The contribution of the e_g bands to the total DOS can easily be identified from the LDA+DMFT spectra, where an additional hump between the quasiparticle peak and the upper Hubbard band appears.

Figure 7(b) shows the local orbitals used for the DMFT calculations together with the corresponding impurity spectral function $A(\omega)$ and the vanadium t_{2g} partial DOS. The latter one is obtained by projecting the lattice Green's function to t_{2g} character using the partial projectors to be intro-

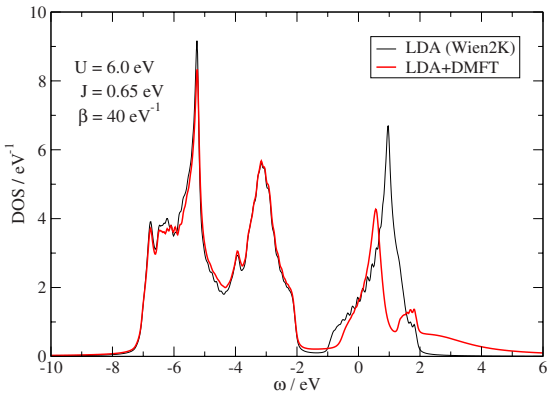

FIG. 8. (Color online) Total DOS for $SrVO_3$, *dp* Hamiltonian (vanadium t_{2g} and oxygen *p*).

duced in Appendix B. The main difference to panel (a) is the absence of the additional e_g character.

Finally, Fig. 8 shows the LDA+DMFT spectral function compared to the LDA density of states, as calculated within the larger energy defined in (ii) above. Since the Wannier functions are more localized, as compared to case (i), the value for the Coulomb interactions has to be adjusted accordingly and we chose a value of $U=6.0$ eV. As can be seen in the figure, ligand states are barely modified by the correlations and the results for the t_{2g}-derived bands are very close to what is seen in the effective low-energy model. The quasiparticle renormalization is $Z=0.57$ in good agreement with the pure t_{2g} treatment discussed before. The results of these calculations correspond to what can be expected on the basis of previously published work, and thus validate our implementation.

APPENDIX B: PROJECTORS FOR PARTIAL DOS

In order to calculate the partial density of states for a given atomic site and particular orbital character (correlated or not) we construct a different type of projectors, which we call $\hat{\mathbf{\Theta}}^{i,\sigma}$. The Wannier operators of Eq. (14) project onto a given Wannier-type orbital. On the other hand, the new set $\hat{\mathbf{\Theta}}^{i,\sigma}$, as we will show, project onto a given orbital of certain character for which we do not apply any orthonormalization process as in the first. Unlike the Wannier projectors, the $\hat{\mathbf{\Theta}}^{i,\sigma}$'s can also project to other orbitals atoms apart from the correlated set.

A given orbital character contributes in the eigenstates through the solutions of the Schrödinger equation inside the spheres $u_l^\sigma(r,E_{l1})Y_m^l\chi_\sigma$, $u_l^\sigma(r,E_{l1})Y_m^l\chi_\sigma$, and $u_l^\sigma(r,E_{l2})Y_m^l\chi_\sigma$ which do not form an orthonormalized basis set. It is more convenient to construct these projectors if the wave function is rewritten in an orthonormal basis set.

In a general form, inside a given sphere we can express $\psi_{\mathbf{k}\nu}^\sigma(\mathbf{r})$ as

$$\psi_{\mathbf{k}\nu}^\sigma(\mathbf{r}) = \sum_{lm} A'_{lm}u_{l1} + \sum_{lm} B'_{lm}\dot{u}_l + \sum_{lm} C'_{lm}u_{l2}, \tag{B1}$$

where we simplify the notation by omitting the angular and spin parts and defining A'_{lm}, B'_{lm}, and C'_{lm} as combined coefficients which are generally *k* dependent and contain the sum over the plane waves and local orbitals. We also define $u_{l1} \equiv u_l(r,E_{l1})$, $\dot{u}_l \equiv \dot{u}_l(r,E_{l1})$, and $u_{l2} \equiv u_l(r,E_{l2})$.

We then rewrite $\psi_{\mathbf{k}\nu}^\sigma(\mathbf{r})$ as a function of a set of orthogonal orbitals $\phi_j(r)$, $j=1,2,3$ as follows:

$$\psi_{\mathbf{k}\nu}^\sigma(\mathbf{r}) = \sum_{lm}\sum_j (A'_{lm}c_{1j}^{lm} + B'_{lm}c_{2j}^{lm} + C'_{lm}c_{3j}^{lm})\phi_j(r). \tag{B2}$$

The coefficients c_{ij}^{lm} are the matrix elements of the square root of the corresponding overlap matrix

$$\mathbf{C} = \begin{pmatrix} 1 & 0 & \langle u_{l1}|u_{l2}\rangle \\ 0 & \langle \dot{u}_l|\dot{u}_l\rangle & \langle \dot{u}_l|u_{l2}\rangle \\ \langle u_{l2}|u_{l1}\rangle & \langle u_{l2}|\dot{u}_l\rangle & \langle u_{l2}|u_{l2}\rangle \end{pmatrix}^{1/2}. \tag{B3}$$

In this way, rewriting Eq. (B2) as

$$\psi_{\mathbf{k}\nu}^\sigma(\mathbf{r}) = \sum_{lm}\sum_j \tilde{c}_j^{lm}\phi_j(r), \tag{B4}$$

the matrix elements of the projector to a given atom with *lm* character finally read as

$$\Theta_{m\nu j}^{i,\sigma}(\mathbf{k}) = \tilde{c}_j^{lm}. \tag{B5}$$

The spectral function of a given atom *i* with orbital character *m* is obtained as

$$A_m^{i,\sigma}(\mathbf{k},\omega) = -\frac{1}{\pi}\mathrm{Im}\left[\sum_{\nu\nu',j} \Theta_{m\nu j}^{i,\sigma}(\mathbf{k})G_{\nu\nu'}^\sigma(\mathbf{k},\omega^+)\Theta_{\nu' m' j}^{i,\sigma *}(\mathbf{k})\right].$$

APPENDIX C: INFLUENCE OF THE ROTATIONAL INVARIANCE OF HUND'S RULE COUPLING IN MULTIORBITAL SYSTEMS

In our DMFT calculations using CTQMC as impurity solver, we restricted the Hund's rule interaction to Ising-type interactions only, although there is no conceptual limitation of the algorithm to this type of interactions. The reason for doing this is of purely technical nature, since in this case one can diagonalize the local problem very efficiently, and furthermore, it enables us to use the so-called segment-picture update scheme,[59] which increases the efficiency of the CTQMC method a lot.

One may now ask how results change if the fully rotational-invariant Hund's rule exchange is taken into account. For this purpose, we study a multiband model Hamiltonian, assuming degenerate bands, no interband hybridizations, and a semicircular density of states. Applying the self-energy functional theory (SFT),[60] we can study the quasiparticle renormalization *Z* as function of interactions *U* and *J*. In this study, we choose the convention of setting the intraorbital Coulomb repulsion to *U* and the interorbital to $U'=U-2J$, and give all energies in units of the single-particle hopping amplitude *t*, i.e., the bandwidth of the DOS is $W=4t$.

In addition to the density-density interactions, we consider also the additional spin-flip and pair-hopping terms of the local Hamiltonian,

$$H_{\mathrm{sf}} = -\frac{J}{2}\sum_{mm'} (c^{\dagger}_{m\uparrow}c_{m\downarrow}c^{\dagger}_{m'\downarrow}c_{m'\uparrow} + \mathrm{H.c.}), \qquad \text{(C1)}$$

$$H_{\mathrm{ph}} = -\frac{J}{2}\sum_{mm'} (c^{\dagger}_{m\uparrow}c^{\dagger}_{m\downarrow}c_{m'\uparrow}c_{m'\downarrow} + \mathrm{H.c.}). \qquad \text{(C2)}$$

We do calculations at $T=0$ and choose the reference system for the SFT framework to consist of one bath degree of freedom for each correlated orbital. Hence, going up to $M=5$ orbitals, we have to diagonalize a local problem consisting of at most ten orbitals.

The upper panel of Fig. 9 shows Z for a three-orbital model at half-filling, $n=3$, for $J=0.1U$. A tremendous reduction in the critical U_c of the metal-to-insulator transition (MIT) is observed, already for Ising-type interactions. This is a well known fact that for multiorbital systems at or close to half-filling, the effect of J should be strongest.[61–63] The inclusion of spin-flip and pair-hopping terms gives rise to two effects. (i) For moderate correlations, $Z \approx 0.6$, these terms lead to a slight reduction in Z, but (ii) the critical U for the MIT is shifted upward. This qualitatively holds also away from half-filling, which can be seen in the lower panel of Fig. 9, where we plotted Z for $n=2$. Although the transition is not of first order anymore, one can again identify two regimes. For moderate correlations, Z *decreases*, whereas close to the transition the spin-flip and pair-hopping terms *increase* the renormalization Z and the critical U_c is pushed to higher values. This is consistent with a numerical renormalization group study for the two-orbital Hubbard model.[62]

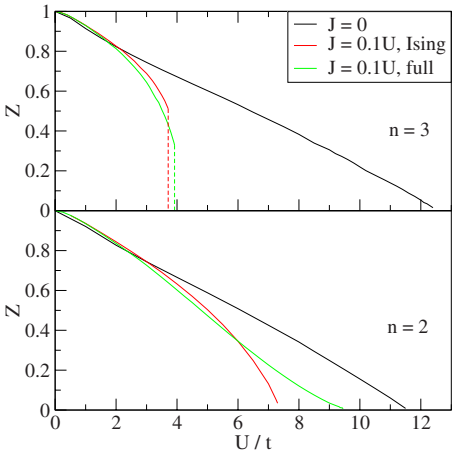

FIG. 9. (Color online) Quasiparticle renormalization Z in a three-orbital Hubbard model. Calculations have been done using a semicircular DOS with bandwidth $W=4t$. Top panel: $n=3$ (half-filling). Bottom panel: $n=2$.

We also considered the case relevant for pnictide materials, i.e., $M=5$, $n=6$, and Z around 0.5. This regime could be realized by setting (i) $U=3.5t$ and $J=0.35t$, which shows a reduction in Z from 0.52 to 0.47 due to spin-flip and pair hopping, or (ii) $U=2t$, $J=0.4t$, giving a reduction from 0.61 to 0.57. In conclusion, this analysis shows that the picture of a moderately correlated metal as argued in Sec. III holds also when a fully rotational-invariant Hund's exchange is considered. For systems close to a MIT, this is no longer true and the spin-flip and pair-hopping terms become crucial.

[1] P. Blaha, K. Schwarz, G. Madsen, D. Kvasnicka, and J. Luitz, *WIEN2k, An Augmented Plane Wave+Local Orbitals Program for Calculating Crystal Properties* (Techn. Universitat Wien, Austria, 2002).
[2] K. Haule, J. H. Shim, and G. Kotliar, Phys. Rev. Lett. **100**, 226402 (2008).
[3] K. Haule and G. Kotliar, New J. Phys. **11**, 025021 (2009).
[4] V. I. Anisimov, D. M. Korotin, M. A. Korotin, A. V. Kozhevnikov, J. Kunes, A. O. Shorikov, S. L. Skornyakov, and S. V. Streltsov, J. Phys.: Condens. Matter **21**, 075602 (2009).
[5] A. O. Shorikov, M. A. Korotin, S. V. Streltsov, S. L. Skornyakov, D. M. Korotin, and V. I. Anisimov, J. Exp. Theor. Phys. **108**, 121 (2009).
[6] V. I. Anisimov, D. M. Korotin, S. V. Streltsov, A. V. Kozhevnikov, J. Kuneš, A. O. Shorikov, and M. A. Korotin, JETP Lett. **88**, 729 (2008).
[7] A. Georges, G. Kotliar, W. Krauth, and M. J. Rozenberg, Rev. Mod. Phys. **68**, 13 (1996).
[8] A. Georges, in *Lectures on the Physics of Highly Correlated Electron Systems VIII*, edited by A. Avella and F. Mancini (American Institute of Physics, New York, 2004); arXiv:cond-mat/0403123 (unpublished).
[9] K. Held, I. A. Nekrasov, G. Keller, V. Eyert, N. Blümer, A. K. McMahan, R. T. Scalletar, T. Pruschke, V. I. Anisimov, and D. Vollhardt, *Quantum Simulations of Complex Many-Body Systems: From Theory to Algorithms*, NIC Series Vol. 10 (John von Neumann Institute for Computing, Jülich, 2002).
[10] S. Biermann, *Encyclopedia of Materials: Science and Technology* (Elsevier Ltd., New York, 2006).
[11] G. Kotliar and D. Vollhardt, Phys. Today **57** (3), 53 (2004).
[12] G. Kotliar, S. Y. Savrasov, K. Haule, V. S. Oudovenko, O. Parcollet, and C. A. Marianetti, Rev. Mod. Phys. **78**, 865 (2006).
[13] E. Pavarini, S. Biermann, A. Poteryaev, A. I. Lichtenstein, A. Georges, and O. K. Andersen, Phys. Rev. Lett. **92**, 176403 (2004).
[14] F. Lechermann, A. Georges, A. Poteryaev, S. Biermann, M. Posternak, A. Yamasaki, and O. K. Andersen, Phys. Rev. B **74**, 125120 (2006).
[15] V. I. Anisimov, D. E. Kondakov, A. V. Kozhevnikov, I. A. Nekrasov, Z. V. Pchelkina, J. W. Allen, S.-K. Mo, H.-D. Kim, P. Metcalf, S. Suga, A. Sekiyama, G. Keller, I. Leonov, X. Ren, and D. Vollhardt, Phys. Rev. B **71**, 125119 (2005).
[16] M. M. Korshunov, V. A. Gavrichkov, S. G. Ovchinnikov, I. A. Nekrasov, Z. V. Pchelkina, and V. I. Anisimov, Phys. Rev. B **72**, 165104 (2005).
[17] I. V. Solovyev, Phys. Rev. B **73**, 155117 (2006).
[18] V. I. Anisimov, A. V. Kozhevnikov, M. A. Korotin, A. V. Lukoyanov, and D. A. Khafizullin, J. Phys.: Condens. Matter **19**, 106206 (2007).
[19] B. Amadon, F. Lechermann, A. Georges, F. Jollet, T. O. Wehling,

and A. I. Lichtenstein, Phys. Rev. B **77**, 205112 (2008).
[20] N. Marzari and D. Vanderbilt, Phys. Rev. B **56**, 12847 (1997).
[21] I. Souza, N. Marzari, and D. Vanderbilt, Phys. Rev. B **65**, 035109 (2001).
[22] A. Liebsch, Phys. Rev. Lett. **90**, 096401 (2003).
[23] A. Sekiyama, H. Fujiwara, S. Imada, S. Suga, H. Eisaki, S. I. Uchida, K. Takegahara, H. Harima, Y. Saitoh, I. A. Nekrasov, G. Keller, D. E. Kondakov, A. V. Kozhevnikov, Th. Pruschke, K. Held, D. Vollhardt, and V. I. Anisimov, Phys. Rev. Lett. **93**, 156402 (2004).
[24] E. Pavarini, A. Yamasaki, J. Nuss, and O. K. Andersen, New J. Phys. **7**, 188 (2005).
[25] I. A. Nekrasov, G. Keller, D. E. Kondakov, A. V. Kozhevnikov, T. Pruschke, K. Held, D. Vollhardt, and V. I. Anisimov, Phys. Rev. B **72**, 155106 (2005).
[26] I. A. Nekrasov, K. Held, G. Keller, D. E. Kondakov, T. Pruschke, M. Kollar, O. K. Andersen, V. I. Anisimov, and D. Vollhardt, Phys. Rev. B **73**, 155112 (2006).
[27] P. Werner, A. Comanac, L. de' Medici, M. Troyer, and A. J. Millis, Phys. Rev. Lett. **97**, 076405 (2006).
[28] K. Haule, Phys. Rev. B **75**, 155113 (2007).
[29] J. C. Slater, Phys. Rev. **92**, 603 (1953).
[30] D. J. Singh, *Plane Waves, Pseudopotentials and the LAPW Method* (Kluwer, Dordrecht, 1994).
[31] E. Sjöstedt, L. Nordström, and D. J. Singh, Solid State Commun. **114**, 15 (2000).
[32] K. S. D. Beach, arXiv:cond-mat/0403055 (unpublished).
[33] V. I. Anisimov, F. Aryasetiawan, and A. I. Lichtenstein, J. Phys.: Condens. Matter **9**, 767 (1997).
[34] A. I. Lichtenstein, M. I. Katsnelson, and G. Kotliar, Phys. Rev. Lett. **87**, 067205 (2001).
[35] E. R. Ylvisaker, W. E. Pickett, and K. Koepernik, Phys. Rev. B **79**, 035103 (2009).
[36] K. Held, Adv. Phys. **56**, 829 (2007).
[37] O. K. Andersen and T. Saha-Dasgupta, Phys. Rev. B **62**, R16219 (2000).
[38] O. K. Andersen, T. Saha-Dasgupta, R. W. Tank, C. Arcangeli, O. Jepsen, and G. Krier, in *Electronic Structure and Physical Properties of Solids: The Uses of the LMTO Method*, Lecture Notes in Physics Vol. 535 (Springer, Berlin, 2000).
[39] E. Zurek, O. Jepsen, and O. K. Andersen, ChemPhysChem **6**, 1934 (2005).
[40] V. Vildosola, L. Pourovskii, R. Arita, S. Biermann, and A. Georges, Phys. Rev. B **78**, 064518 (2008).
[41] F. Aryasetiawan, M. Imada, A. Georges, G. Kotliar, S. Biermann, and A. I. Lichtenstein, Phys. Rev. B **70**, 195104 (2004).
[42] T. Miyake and F. Aryasetiawan, Phys. Rev. B **77**, 085122 (2008).
[43] T. Miyake, F. Aryasetiawan, and M. Imada, arXiv:0906.1344 (unpublished).
[44] K. Nakamura, R. Arita, and M. Imada, J. Phys. Soc. Jpn. **77**, 093711 (2008).
[45] T. Miyake, L. Pourovskii, V. Vildosola, S. Biermann, and A. Georges, J. Phys. Soc. Jpn. **77**, 99 (2008).
[46] W. Malaeb, T. Yoshida, T. Kataoka, A. Fujimori, M. Kubota, K. Ono, H. Usui, K. Kuroki, R. Arita, H. Aoki, Y. Kamihara, M. Hirano, and H. Hosono, J. Phys. Soc. Jpn. **77**, 093714 (2008).
[47] E. Z. Kurmaev, R. G. Wilks, A. Moewes, N. A. Skorikov, Y. A. Izyumov, L. D. Finkelstein, R. H. Li, and X. H. Chen, Phys. Rev. B **78**, 220503(R) (2008).
[48] D. H. Lu, M. Yi, S.-K. Mo, J. G. Analytis, J.-H. Chu, A. S. Erickson, D. J. Singh, Z. Hussain, T. H. Geballe, I. R. Fisher, and Z.-X. Shen, Physica C **469**, 452 (2009).
[49] M. Imada, A. Fujimori, and Y. Tokura, Rev. Mod. Phys. **70**, 1039 (1998).
[50] A. Fujimori, I. Hase, H. Namatame, Y. Fujishima, Y. Tokura, H. Eisaki, S. Uchida, K. Takegahara, and F. M. F. de Groot, Phys. Rev. Lett. **69**, 1796 (1992).
[51] M. Onoda, H. Ohta, and H. Nagasawa, Solid State Commun. **79**, 281 (1991).
[52] K. Maiti, D. D. Sarma, M. Rozenberg, I. Inoue, H. Makino, O. Goto, M. Pedio, and R. Cimino, Europhys. Lett. **55**, 246 (2001).
[53] K. Maiti, Ph.D. thesis, IISC, Bangalore, 1997.
[54] I. H. Inoue, I. Hase, Y. Aiura, A. Fujimori, Y. Haruyama, T. Maruyama, and Y. Nishihara, Phys. Rev. Lett. **74**, 2539 (1995).
[55] T. Yoshida, K. Tanaka, H. Yagi, A. Ino, H. Eisaki, A. Fujimori, and Z.-X. Shen, Phys. Rev. Lett. **95**, 146404 (2005).
[56] H. Wadati, T. Yoshida, A. Chikamatsu, H. Kumigashira, M. Oshima, H. Eisaki, Z. X. Shen, T. Mizokawa, and A. Fujimori, Phase Transitions **79**, 617 (2006).
[57] R. Eguchi, T. Kiss, S. Tsuda, T. Shimojima, T. Mizokami, T. Yokoya, A. Chainani, S. Shin, I. H. Inoue, T. Togashi, S. Watanabe, C. Q. Zhang, C. T. Chen, M. Arita, K. Shimada, H. Namatame, and M. Taniguchi, Phys. Rev. Lett. **96**, 076402 (2006).
[58] Even though comparisons with x-ray absorption spectroscopy have been attempted it is not clear that the low-energy description by a pure t_{2g} model is still valid at these energies. Note in particular that in this energy region overlaps with the e_g states, split off by the cubic crystal field, could come into play.
[59] P. Werner and A. J. Millis, Phys. Rev. B **74**, 155107 (2006).
[60] M. Potthoff, Eur. Phys. J. B **32**, 429 (2003).
[61] Y. Ono, M. Potthoff, and R. Bulla, Phys. Rev. B **67**, 035119 (2003).
[62] T. Pruschke and R. Bulla, Eur. Phys. J. B **44**, 217 (2005).
[63] K. Inaba, A. Koga, S.-I. Suga, and N. Kawakami, Phys. Rev. B **72**, 085112 (2005).